Cell Biochem Biophys
DOI 10.1007/s12013-012-9397-3

ORIGINAL PAPER

# Extracting the Stepping Dynamics of Molecular Motors in Living Cells from Trajectories of Single Particles

**Augusto Bruno · Luciana Bruno · Valeria Levi**



**Abstract** Molecular motors are responsible of transporting a wide variety of cargos in the cytoplasm. Current efforts are oriented to characterize the biophysical properties of motors in cells with the aim of elucidating the mechanisms of these nanomachines in the complex cellular environment. In this study, we present an algorithm designed to extract motor step sizes and dwell times between steps from trajectories of motors or cargoes driven by motors in cells. The algorithm is based on finding patterns in the trajectory compatible with the behavior expected for a motor step, i.e., a region of confined motion followed by a jump in the position to another region of confined motion with similar characteristics to the previous one. We show that this algorithm allows the analysis of 2D trajectories even if they present complex motion patterns such as active transport interspersed with diffusion and does not require the assumption of a given step size or dwell period. The confidence on the step detection can be easily obtained and allows the evaluation of the confidence of the dwell and step size distributions. To illustrate the possible applications of this algorithm, we analyzed trajectories of myosin-V driven organelles in living cells.

**Keywords** Single particle tracking · Molecular motors · Stepping dynamics · Dwell time · *Xenopus* melanophores

A. Bruno · L. Bruno
Departamento de Física, Facultad de Ciencias Exactas y Naturales, Universidad de Buenos Aires, Pabellón 1, Ciudad Universitaria, CP 1428 Ciudad de Buenos Aires, Argentina

A. Bruno · V. Levi (✉)
Departamento de Química Biológica, Facultad de Ciencias Exactas y Naturales, Universidad de Buenos Aires, Ciudad Universitaria, CP 1428 Ciudad de Buenos Aires, Argentina
e-mail: vlevi12@gmail.com

## Introduction

Molecular motors play important roles in a wide variety of cellular processes from segregation of chromosomes during mitosis to vesicular transport in the cell cytoplasm. Motors attach to cytoskeleton polymers, i.e., actin filaments and microtubules, and move in a stepwise manner along these tracks converting the energy provided by ATP hydrolysis into mechanical work (see for example, [1]).

The molecular mechanism involved in the motor movement along cytoskeleton tracks has been extensively studied mainly by single molecule techniques. The force of molecular motors was measured by optical trapping ranging between 1 and 7 pN [2–5]; this technique was also used to dissect the motor reaction cycle (see for example, [6, 7]). On the other hand, single particle tracking (SPT) with nanometer accuracy have been used to study properties of motors such as the stepping mechanism of single [8, 9] or small ensembles of motors [10–12] and the influence of the environment and cytoskeleton tracks organization in the motor dynamics [13, 14].

However, the functional properties of motors in their natural environment cannot be directly extrapolated from these in vitro measurements. The cell cytoplasm behaves as a complex, viscoelastic fluid [15] which exerts drag on motor molecules. Moreover, it has been recently demonstrated that the dynamics of the cytoskeleton also affect the motion of organelles driven by motors [16, 17] and that active motion along cytoskeleton tracks is usually interspersed by periods of diffusion [18]. On the other hand, motor activity is finely regulated in living cells by other proteins which are not present in in vitro determinations [19, 20].

Current efforts are oriented to characterize the biophysical properties of molecular motors in the complex

Published online: 20 July 2012

cellular environment. Two main strategies have been followed with this aim; either tracking micrometer-sized cargoes transported by motors and inferring the motion of the motors from this data or studying directly the motion of single motors labeled with bright fluorescent probes (reviewed in [21]).

We and others have demonstrated that it is possible to detect single steps of motor proteins in living cells by tracking organelles transported along cytoskeleton tracks [22–25]. These reports show that the step sizes of myosin-V and kinesin-2 in living cells are 36 and 8 nm, similar to what it is observed in in vitro conditions [22–24]. On the other hand, myosin-VI performs steps of 29 and 15 nm in living cells with a dwell time of ~30 ms [25]. Importantly, the small step of this motor has not been observed in in vitro assays. Watanabe et al. also determined that the characteristic dwell times of kinesin- and dynein-driven cargoes were 5 and 7.5 ms, respectively [25].

Nan et al. [26] improved the temporal resolution to the microsecond range and tracked gold nanoparticles-containing endosomes which were further detected in a darkfield microscopy setup. They reported that while kinesin driven endosomes present clear 8 nm steps, dynein-driven endosomes can take either 8 nm or longer steps not observed before in living cells. This result was expected since cytoplasmic dynein present different step sizes under different loads in in vitro conditions [2]. They could also measure the in vivo rising time of the steps ranging from 100 μs to a few milliseconds which is at least twice as slow as the in vitro rising time. In the same direction, we have estimated the rising time of myosin-V driven organelles on 20–80 ms [23]. The motion of single kinesin and myosin molecules in the cytoplasm of living cells has also been studied by using quantum dots and tandems of fluorescent proteins to label the motor molecules avoiding studying the motor properties by following the motion of their cargoes [27–30].

Taken together, these studies showed that important biophysical properties of motors such as the distributions of step size, dwell time, velocity, and run length can be studied by SPT and opened the possibility of analyzing the detailed molecular mechanisms of motor transport in the cytoplasm of living cells.

Unfortunately, the analysis of the data obtained in SPT experiments is often performed by arbitrary selecting regions of the trajectories showing curvilinear motion, linearizing them and picking up steps from the distance vs. time plot by eye examination, pairwise analysis or with algorithms designed for in vitro experiments in which motors move processively along a linear track (see references in [31]). As we mentioned before, these are not the conditions in which transport develops in living cells.

In this study, we present a new algorithm designed to extract step size ($L$) and dwell time ($D_T$) distributions from trajectories of single organelles or single motors in living cells. This step-finder algorithm presents clear advantages with respect to previous methods used for the analysis of in vitro experiments when analyzing trajectories of motors or cargoes in living cells. Specifically, it allows the analysis of 2D trajectories without assuming motion along a linear path as in vitro algorithms. Moreover, it can be used to analyze trajectories presenting active transport and diffusion and does not assume given values of $L$ or $D_T$. We show that the confidence on the step detection can be easily obtained and allow the evaluation of the confidence of the overall experimental distributions of $L$ and $D_T$. To illustrate the possible applications of this algorithm to studies of transport, we analyzed trajectories of myosin-V driven organelles in living cells.

## Materials and Methods

### Melanophore Cell Culture and Imaging

Immortalized *Xenopus laevis* melanophores were cultured as described in [32]. In order to track the movement of individual organelles, the number of melanosomes in cells was reduced by treatment with phenylthiourea [33]. To study transport along actin filaments, the cells were incubated at 0 °C for 30 min with 10 μM nocodazole to depolymerize microtubules [23].

For microscopy measurements, cells were grown for 2 days on 25-mm round coverslips. Before observation, the coverslips were washed in serum-free 70 % L-15 medium and mounted in a custom-made chamber specially designed for the microscope. All the measurements were performed at 21 °C.

### Tracking Experiments

SPT experiments of melanosomes moving along actin filaments were carried out in a Olympus IX70 microscope adapted for SPT using a 60× oil-immersion objective (numerical aperture = 1.25) under illumination with a tungsten–halogen lamp. A cMOS camera (Pixelink, Ottawa, ON, Canada) was attached to the video port of the microscope for imaging the cells at a speed of 50 frames/s.

Trajectories of melanosomes were recovered from the movies registered as described above using the pattern-recognition algorithm described in [34]. This algorithm is included in the program Globals for Images developed at the Laboratory for Fluorescence Dynamics (UCI, Irvine, CA). The program, which also contains some of the tools used for trajectory analysis, can be downloaded from the Laboratory for Fluorescence Dynamics website (www.lfd.uci.edu).

### Numerical Simulations and Data Analysis

Numerical codes were written and run in Matlab environment (The Mathworks, Natick, MA).

The bin size of histograms was determined following the criteria proposed previously [35].

## Results and Discussion

### The Step-Finder Algorithm

Figure 1a represents a trajectory of a melanosome transported along actin filaments by myosin-V. This trajectory presents periods of motion which characteristics seems compatible with active transport interspersed with regions in which the organelles are probably detached from the actin tracks and perform a complex diffusive process in which other forces such as remodeling and reorganization of the cytoskeleton play an important role [18, 36]. As can be observed from this representative trajectory, motion of motor-driven organelles in the cell cytoplasm is usually very complex and cannot be analyzed by only considering active transport along curvilinear cytoskeleton tracks.

To obtain quantitative information regarding the stepping dynamics of motors in the cell cytoplasm, we constructed an algorithm that allows extracting motor steps and dwell times between steps from the whole trajectory without the requirements of arbitrarily selecting regions in which active transport is presumed and assuming an underlying shape for the cytoskeleton track.

The algorithm is based on finding patterns in the trajectory compatible with the behavior expected for a motor step, i.e., a region of confined motion followed by a jump in the position to another region of confined motion with similar characteristics to the previous one. The radius of these regions of confined motion is related to the fluctuations of the position of the organelle or motor given by thermal jittering in the intracellular medium [37] and the error on the position determination which is given by the particle tracking algorithm and the experimental noise [38]. We define the parameter $\sigma$ as the standard deviation of the organelle position during these periods of constrained motion. According this definition, the radius of the confined regions of diffusion is $\sim 2\sigma$.

Figure 1b schematizes the general procedure followed to localize the regions of confined motion. The routine starts by setting a sliding circle of radius $\delta$ at the position corresponding to the coordinates of the first data point of the trajectory. Then, the program analyzes whether the consecutive point of the trajectory falls inside or outside of this circle. In the first case, the program re-centers the circle to the average position between both data points and analyzes the subsequent points in the trajectory recalculating the position of the circle center after each data point analysis. This procedure continues until two consecutive data points fall outside the circle. In that condition, the program classifies this segment of the trajectory as a hypothetic dwell and saves the number of data and coordinates of the circle. Single data points outside the circle but belonging to a trajectory segment included in a dwell period are also computed as part of this hypothetic dwell.

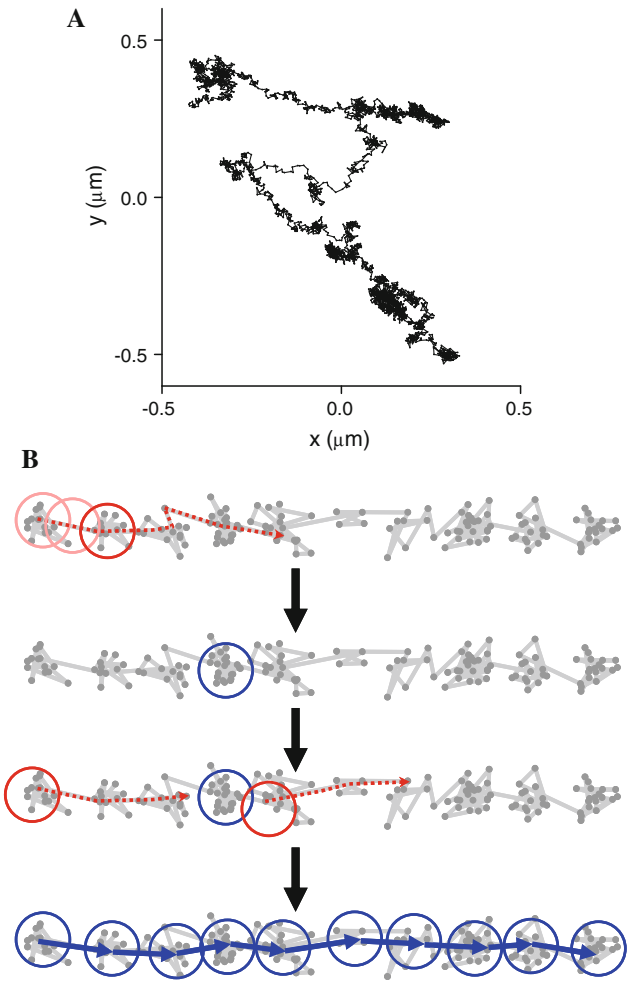


**Fig. 1** Analysis of motor stepping in living cells. **a** Representative trajectory of melanosomes moving along actin filaments by the action of myosin-V. The trajectory lasted for 80 s. **b** Simulated trajectory of a particle undergoing fixed steps with variable $D_T$ and Gaussian-distributed noise with standard deviation equal to 20 % of the step size. The *pink circles* illustrate different positions of the sliding circle which is represented in *red* (*top*). The region corresponding to the hypothetic dwell period containing the greatest number of data points is represented in *blue* (*middle top*). The trajectory is split in two segments after removing from the analysis the data contained in the detected dwell (*blue*) and both segments are further analyzed as before (*middle bottom*). The analysis results on the detection on the dwell regions (*blue circles*). Steps (represented with *arrows*) are then calculated as the distance between continuous dwells periods (*bottom*) (Color figure online)

The program then moves the circle to the position corresponding to the second data point and repeats the analysis described before. This procedure is performed with the rest of the points of the trajectory. Once this is done, the program sorts the hypothetic dwells according to the number of data included in them and saves the coordinates of the dwell period containing the highest number of data; these points are excluded from further analysis. The procedure resumes as before with the two trajectory segments remaining after extracting the first dwell period. These iterations are necessary since removing a segment of the trajectory may affect the number of data and center of mass of the hypothetic dwells adjacent to the removed segment. The procedure is iteratively repeated and results in the detection of dwell periods in the trajectory; steps are then calculated as the distance between the centers of two continuous dwell periods.

To initiate the step-finder routine, the user only needs to set values for the minimum number of data points to be considered as a dwell period ($N_{crit}$) and $\delta$.

## Comparative Performances of the Step-Finder Method and Previous Algorithms

In a previous work, Carter et al. [31] compared different algorithms of steps detection designed for the analysis of processive motion along one dimensional (1D) tracks and concluded that the $\chi^2$ minimization method designed by Kerssemakers et al. [39] presented the highest performance. Briefly, the $\chi^2$ method starts by fitting a single large step to the distance vs. time plot obtained from the trajectory and calculates the $\chi^2$ for this initial fitting. Subsequent steps are found by fitting new steps, each time selecting the most prominent one first. This leads to a series of "best" fits that differ only by one step. Each best fit in the series is afterward compared to a "counter fit" that has an equal number of steps as the original one but with step locations in between the step locations found by the best fit. The final fit of the data is considered as the one that gives the highest value for the ratio between the $\chi^2$ of the counter fit to the best fit. This method can also be extended to analyze curvilinear trajectories. To do that, the shape of the underlying filament is previously calculated by using, for example, a polynomial fit and the coordinates of the particle along the filament are used as input for the $\chi^2$ method. This approach was followed by Pierobon et al. [28].

We compared the performance of the step-finder algorithm with that described in Ref. [39]. With this aim, we simulated 1D trajectories of particles performing steps using conditions identical to those assayed before [31] and analyzed the capability of our algorithm to detect the simulated steps. To quantify the performance of the algorithms, we followed the analysis of Carter et al. [31] and used three different performance indicators: the total number of recovered steps, the number of steps correctly detected, and the number of steps correctly detected which sizes equal that of the simulated step ("correct size" steps).

For this analysis, we considered that a given step is correctly detected if the position of the center of the first circle agreed with the position of the simulated particle before the step within a 37.5 % bound confidence. Also, the step size is considered correct if the distance between the two circle centers did not differ from the simulated step within 37.5 % (this criterion is used in Ref. [31]).

Figure 2 shows that the number of steps detected by our algorithm is within 90–120 % of the total steps in every assayed condition. However, both the number of correct steps and correct size steps decreased with the noise showing that false steps are probably detected at high noise levels. Figure 2a–c shows that the performance of the algorithm presented in this study was similar to that of Kerssemakers et al. [39] in every assayed condition of noise/$L$. On the other hand, Fig. 2d shows that our algorithm presented a slightly worst performance as a function of $D_T$. We found that the reduction of the performance was due to the detection of false, intermediate steps within dwells. In these conditions, the Kerssemakers method will have a better performance for noise/step ratios lower than the limit value assayed in this study.

In summary, Fig. 2 shows that the step-finder algorithm presented in this article worked as well as the algorithm designed by Kerssemakers et al. [39] when analyzing 1D trajectories of motors with fixed $D_T$ and $L$, within the assayed ranges of noise/$L$ ratios and $D_T$.

## Global Plot of Step Detection Efficiency

In order to explore how the parameters required in the step-finder routine, i.e., $N_{crit}$ and $\delta$ affect the performance of the algorithm, we first simulated trajectories in which $D_T$ and noise were independently varied in a wide range allowing us to measure the performance of the algorithm in 30 different conditions.

In these simulations, $L$ was considered equal to 1 in arbitrary units and $D_T$ ranges between 2 and 24 also in arbitrary units. Zero-centered Gaussian-distributed noise with standard deviation ranging from 0.2 to 0.5 was added to each simulated trajectory. For every studied condition, we simulated trajectories with 100 steps and analyzed the data with the step-finder algorithm considering different $\delta$ and $N_{crit}$ values.

To quantify the performance of the algorithm, we defined the efficiency or confidence of step detection ($E$) as the ratio of the number of steps which position and size are accurately detected by the algorithm within a 37.5 % bound confidence (i.e., "correct size steps") to the total number of detected

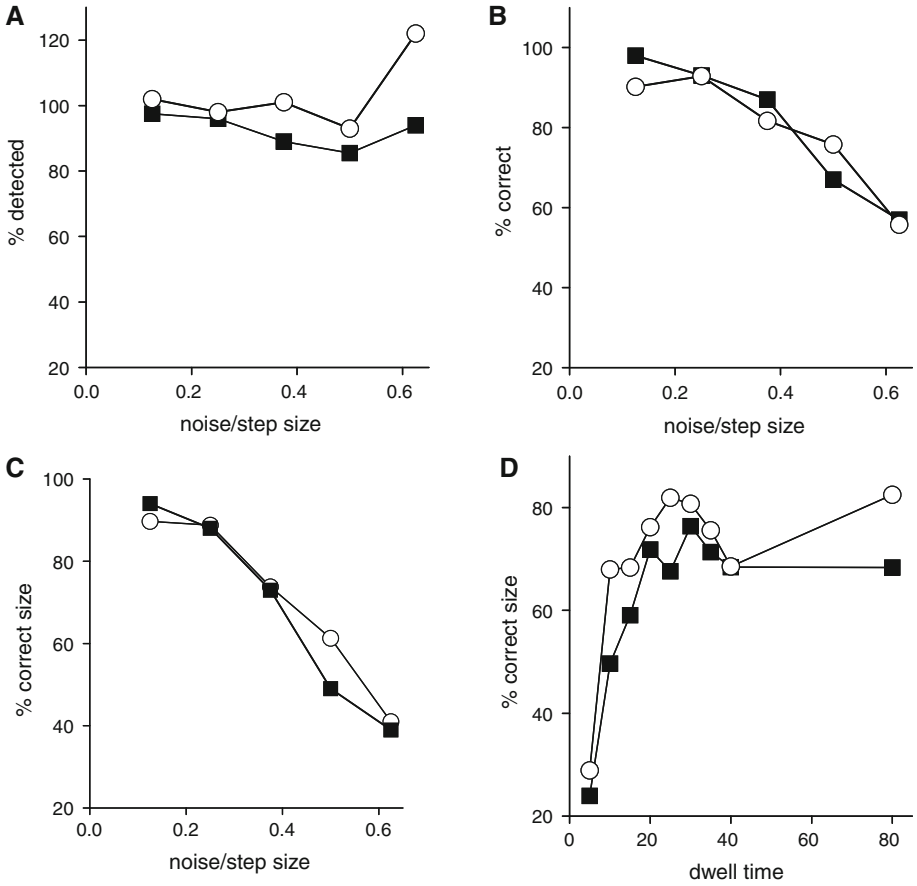


**Fig. 2** Performance of the step-finder algorithm. Trajectories of particles performing 600 steps of 8 nm were simulated considering an exponential decay distribution for $D_T$ with $\tau = 24$ data points and Gaussian noise ranging 1–5 nm. The data was analyzed by using the algorithms described in this study (*black square*) and that designed by Kerssemakers et al. (*circle*) and the performance of the algorithms were determined quantifying **a** detected steps, **b** correct steps, and **c** "correct size" steps. **d** The number of "correct size" steps recovered by the step-finder algorithm was also evaluated as a function of $\tau$ (in units of data points). For this analysis, we simulated and analyzed trajectories consisting of 200 steps of 8 nm with Gaussian noise of 3 nm. The $N_{crit}$ and $\delta$ values used to analyze the data with the step-finder algorithm were chosen using the global plot of step detection efficiency presented in Fig. 3

steps. This parameter ranges from 0 to 1 and is a direct measure of the goodness of the recovered steps. The straightforward evaluation of the ratio of recovered to simulated steps is not a correct indicator of the performance since this ratio can be high even if the size and the position of the recovered steps in the trajectory are not the correct ones. Moreover, an overestimation of the number of steps in the trajectory may result in ratios of recovered/simulated steps higher than 1, while the value of $E$ will decrease in this particular situation. One disadvantage of this ratio is that $E$ can be as high as 1 even if the algorithm does not detect all the simulated steps.

Figure 3 shows the global plot of step detection efficiency (GPS) in four different assayed conditions. Noticeable, the maximum value of $E$ in each assayed condition was achieved with different values of $N_{crit}$ and $\delta$. Moreover, while $E$ can be as high as 1 when $\sigma$ is low (Fig. 3b), the average efficiency attained for $\sigma$ equal to 30 % of the step size was reduced to $\sim$80 % (Fig. 3d) as was shown before. In most of the assayed conditions, we found that efficiency higher than 50 % could be attained with $\delta$ values near $1.8\sigma$ thus this value can be considered as the starting circle radius for the analysis of experimental data.

The figure shows that steps with variable $D_T$ or $\sigma/L$ ratio were recovered with different efficiencies. As we mentioned in the "Introduction" section, this may be expected for motors in living cells and therefore it is required to consider this bias in the step-finder routine.

## General Procedure for Recovering Step Size and Dwell Time Information in Complex Trajectories

In the previous section, we showed that the efficiency of the step-detection algorithm depended on the stepping properties of the motors and the selected values for the parameters used in the routine. Therefore, we decided to use the data contained in the GPS to assign a confidence value to each step detected by the algorithm. In this section, we describe the general procedure followed in the analysis of experimental data.

In order to estimate $\sigma$ from the data we followed two different procedures: either we applied a short-pass FFT filter to the trajectories of the organelles/motors and obtained the standard deviation of the filtered data or calculated $\sigma$ as the standard error of the particle position determination by tracking immobile particles in the

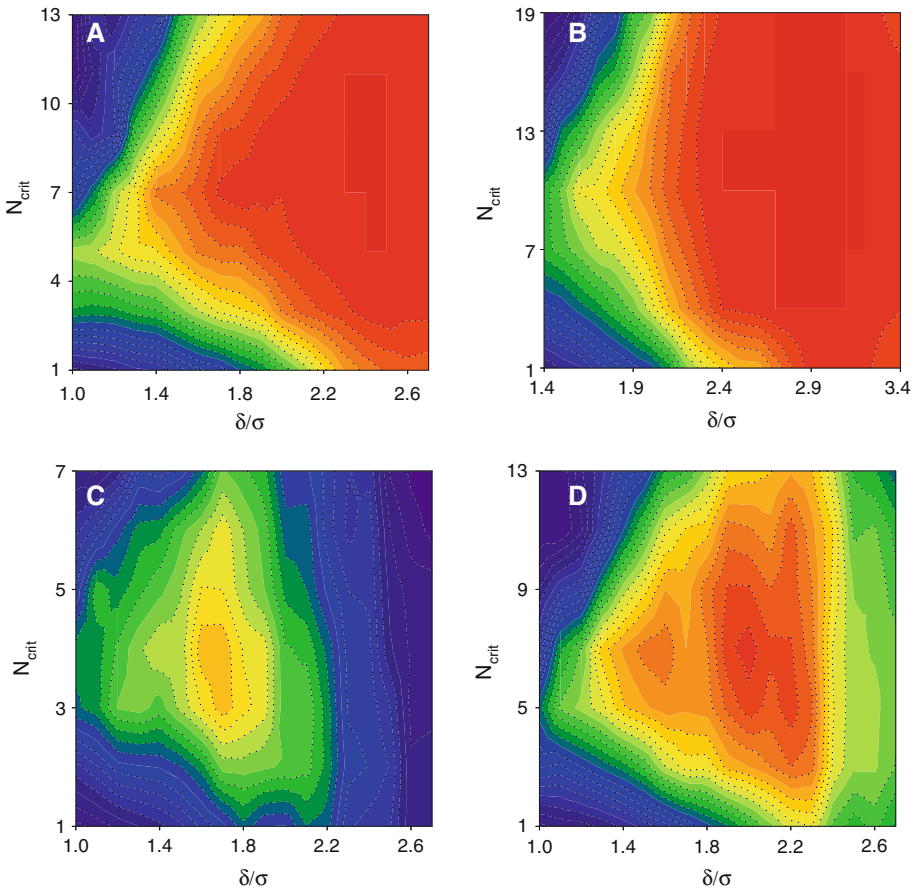


**Fig. 3** Global plot of step detection efficiency. Trajectories of particles performing 100 steps with $L = 1$ and $D_T$ ranging between 2 and 32 (all in arbitrary units) were simulated as described before. Zero-centered Gaussian noises were added to each simulated trajectory, with $\sigma$ values ranging 0.2–0.5. Each trajectory was analyzed with the step-finder algorithm using different values of $\delta$ and $N_{crit}$. The efficiency of step detection is represented in pseudocolor from 0 (*blue*) to 1 (*red*) as a function of the ratio $\delta/\sigma$ and $N_{crit}$ for the following conditions: **a** $D_T = 16$ and $\sigma/L = 0.2$; **b** $D_T = 24$ and $\sigma/L = 0.2$; **c** $D_T = 8$ and $\sigma/L = 0.3$, and **d** $D_T = 16$ and $\sigma/L = 0.3$ (Color figure online)

conditions used for the SPT experiments with motors. In this last analysis, the radius may be slightly underestimated since it only evaluates fluctuations in the position due to the experimental noise; however, we found that both procedures worked equally well in the analysis of our experimental data (not shown). Once $\sigma$ was estimated we input in the program the trajectory data and the values of $\delta$ and $N_{crit}$ selected by the user.

The output of this first part of the routine is a matrix that contains the position of the detected dwell periods, the number of data points included in each dwell and the value of $L$. The program then calculates for each detected step the ratio $\sigma/L$ and computes the lowest dwell time within the two that define the step. These values and the parameters of the program used to detect the steps are considered as the input in the GPS to assign a confidence value to each step. The user then arbitrarily chooses a threshold value for the confidence to decide whether each recovered step will be computed as a real step or not.

For example, if we analyze a trajectory with $\sigma = 10$ nm considering $\delta/\sigma = 1.8$ and $N_{crit} = 5$ and the recovered $L$ and $D_T$ were 33 and 8, respectively. Figure 3c shows that the step confidence is $\sim$60 %. This step is rejected if the confidence threshold were set at 60 %.

If the threshold value is very low, multiple false steps may be included in the further analysis while if the confidence is high, the output will consist in a small number of very precise steps. It is important to mention that confidence threshold extremely high will biased the distribution toward long steps since short steps presents higher values of $\sigma/L$.

Finally, the program builds the histograms of $D_T$ and $L$ for the high-confidence steps, and provides a plot of the $x$–$y$ original trajectory with vectors positioned at the detected steps. As shown below, this last graph can be useful in case the user would like to correlate the steps properties with the general characteristics of the trajectory. Importantly, only dwell periods located between two continuous steps are included in the $D_T$ histogram since these are the only well-defined dwells.

These histograms can also be used to check if the values selected for $N_{crit}$ and $\delta$ were the optimal ones. For example, if the obtained average $D_T$ was equal to 20 (in arbitrary units) and the average $\sigma/L$ was 0.2 using a $N_{crit} = 2$, Fig. 3a shows that the algorithm would have worked better using $N_{crit} \sim 10$. Then, the user can re-run the program using this $N_{crit}$ in order to optimize the confidence of the recovered steps.

Figure 4 shows the general procedure followed by the step-finder program applied to a simulated 2D trajectory of

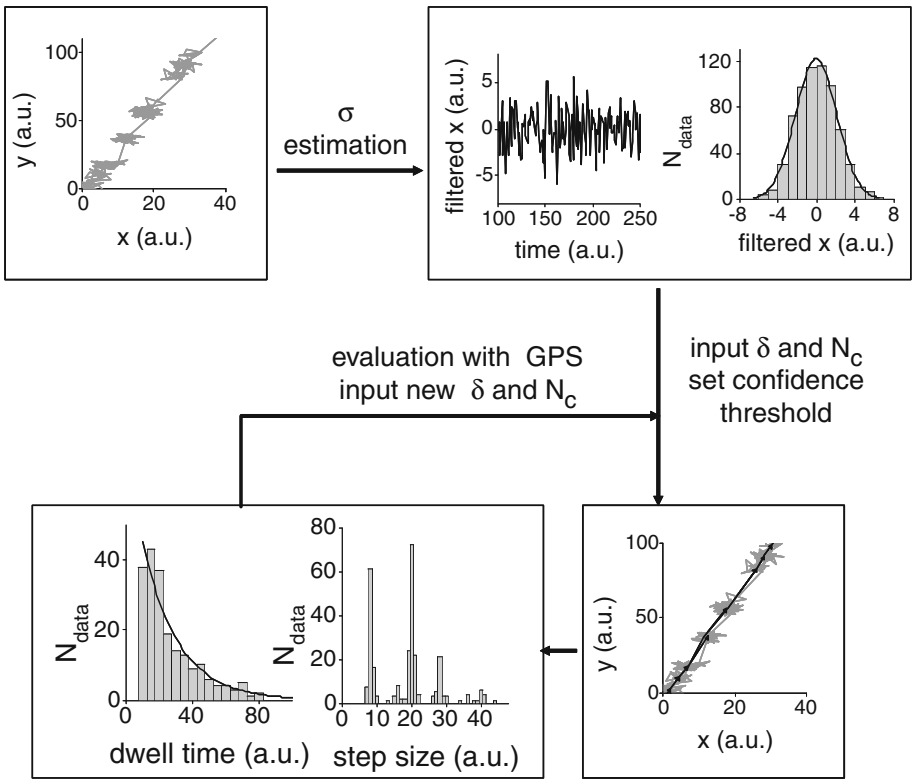


**Fig. 4** Analysis of step size and dwell distributions in complex trajectories. 2D trajectories of a particle undergoing steps of 8 or 20 arbitrary units with equal probability and $D_T$ exponentially distributed were simulated and analyzed with the step-finder algorithm. A small region of a representative trajectory is shown as input. The trajectory was filtered using a high-pass filter with a cutoff frequency equal to 0.05 and the distribution of the filtered data was fitted with a Gaussian function with waist $= 2.15 \pm 0.08$. The step-finder algorithm was initially run using $\delta = 4$ and $N_{crit} = 4$ and a confidence criteria of 80 %. The initial dwell time distribution recovered from this analysis was used to determine that the optimal value for $N_{crit}$ was 7. As an example, the steps determined in the presented region of the trajectory are shown as *black arrows*. The histograms of $L$ and $D_T$ obtained for a trajectory of $\sim$250 of each 8-steps and 20-steps are shown as output of the algorithm. The $D_T$ distribution followed an exponential decay function with $\tau = 21 \pm 2$ (*black line*)

a particle presenting steps of either 8 or 20 arbitrary units (a.u.) randomly distributed along the trajectory. $D_T$ was considered to be exponentially distributed with a characteristic $\tau = 24$ in arbitrary time units with 1 unit corresponding to the time resolution of the simulated experiment. After the simulation, we added to each data point of the trajectory Gaussian-distributed noise with a standard deviation of two arbitrary units.

The figure shows a small region of a representative simulated trajectory and the estimation of $\sigma$ obtained by FFT filtering of one of the coordinates of the particle as a function of time. The distribution of filtered positions was fitted with a Gaussian function and $\sigma$ was obtained as the standard deviation of this distribution. In this particular case, we obtained $\sigma = 2.15 \pm 0.08$. As we showed before, the optimal efficiency in most conditions can be achieved with $\delta \cong 1.8\sigma$ and therefore, this value can be input as the initial $\delta$.

After setting the initial values of $N_{crit}$ and $\delta$ and the confidence criteria, the routine output a plot of the steps as vectors on the trajectory and the histograms of $D_T$ and $L$. Noticeable, in this particular case the step size distribution presented two major peaks at 8 and 20 a.u. and a small peak at 28 a.u. that may be due to the detection of $8 + 20$ consecutive steps with an undetected short-dwell period. The $D_T$ distribution was fitted to an exponential decay function obtaining a characteristic $\tau = 21 \pm 2$ which agreed well with the simulated dwell distribution.

## Application of the Step-Finder Algorithm to Trajectories of Myosin-V Driven Melanosomes

To show the possible applications of the step-finder program described in this study and illustrate the simplicity of the resulting analysis, we studied the motion of myosin-driven melanosomes in cells in which the microtubule network have been depolymerized [23]. It is important to mention that melanosomes are extremely rigid and do not deform significantly in the cellular environment [40].

Movies of regions of the cells were recorded from which a total of 50 trajectories of melanosomes moving along actin filaments were obtained using the pattern-recognition algorithm.

Since trajectories of motors in living cells may include periods of diffusion and switches in direction (Fig. 1a), we also incorporated in the program a routine for filtering the stepping data obtained before using as a criteria the relative angle between two continuous steps. If the detected steps are supposed to be part of a processive region of the trajectory, we would expect a low angle between these step vectors. Therefore, the user may also input in the program an arbitrary maximum value for this critical angle between continuous steps to further filter the data.

Figure 5 shows a representative trajectory of a myosin-driven melanosome and the output of the step-finder algorithm. The program detected several steps in this trajectory with confidences higher than 70 % which were further filtered considering a critical angle of 60°.

Figure 6 shows the histograms of $L$ and $D_T$ constructed from the analysis of the trajectories using the same confidence and critical angle values used for the analysis of the trajectory showed in Fig. 5.

The step size histogram could be described as the sum of two Gaussian distribution functions centered at 37.1 ± 0.6 nm and 72 ± 4 nm with standard deviation of 11.6 ± 0.6 nm. The second peak of the distribution probably reflects two continuous 37 nm steps separated by a short dwell. The center of the first peak of the distribution agree well with the predicted step size of myosin obtained by our and other groups [23, 28, 29] showing that the step size of myosin-V in vivo is identical to that determined in vitro [5]. As far as we know, there are no reports claiming that the actin-dependent motor myosin-V works in multi-motor arrays as microtubule-dependent motors.

The $D_T$ data was examined using a mean residual plot analysis [41] and determined to be exponential for dwell times above 200 ms. We estimated the time constant of the exponential distribution as $\tau = \overline{x|_{x>u}} - u$, where $\overline{x|_{x>u}}$ is the mean value of the excess distribution above a threshold and $u$ is the value of the threshold [41]. We verified that $\tau$ remained constant as the threshold was increased.

We determined for the first time the $D_T$ distribution of myosin-V driven melanosomes obtaining a characteristic time for the dwell period of 150 ms.

This characteristic dwell time is longer than the 60–80 ms dwell time determined for the same motor labeled with Qdots in Cos-7 and Hela cells [28, 29]. Taking into account that

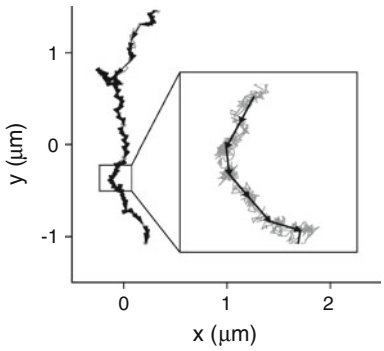


**Fig. 5** Extracting the stepping dynamics of myosin-V driven melanosomes. A representative trajectory of a melanosome driven by myosin-V in living melanophore cells was analyzed with the step-finder algorithm using $N_{crit} = 7$ and $\delta = 21$ nm and a threshold confidence of 80 % obtaining the steps observed with *black arrows*. The trajectory lasted for 80 s. The accuracy on melanosome position determination was 10 nm

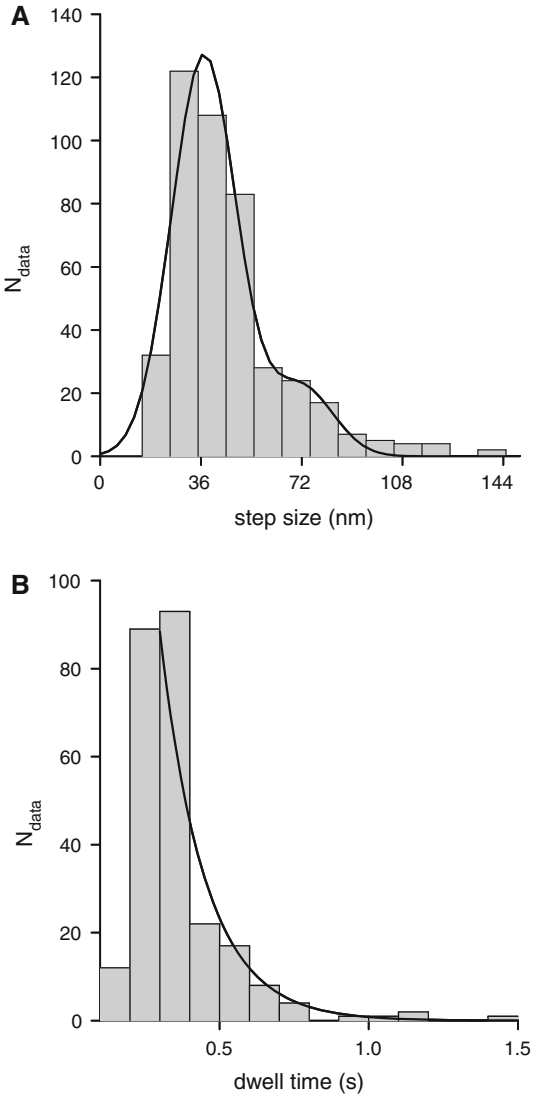


**Fig. 6** Characterization of the stepping properties of myosin-V driven melanosomes. Fifty trajectories of melanosomes transported by myosin-V were obtained as described in "Materials and Methods" section and analyzed with the step-finder algorithm using $N_{crit} = 7$ and $\delta = 18$ nm. **a** Step size distribution. The data was fitted with the sum of two Gaussian functions with the best fitting parameters indicated in the text (*continuous line*). **b** Dwell time distribution. The data followed an exponential decay behavior above 200 ms. The time constant was 150 ± 20 ms (*continuous line*)

melanosomes radius is ~10 times bigger than Qdots radius [32, 42], this result may reflect the relevance of the cargo size and therefore of the drag force on motor stepping dynamics in living cells. This longer dwell period may also be a consequence of the drag introduced by the interaction of melanophilin molecules attached to melanosomes with actin filaments [43]. It is important to mention that the average speed of the myosin motor reported for the motor labeled with Qdots (~700 nm/s, [28]) is significantly higher than that observed for melanosomes driven by myosin-V (~80 nm/s, [18, 44]) also supporting that the drag force in our experimental condition is higher.

## Final Remarks

In this study, we presented a new algorithm designed to extract quantitative information of the stepping dynamics of molecular motors in living cells. We believe that this new routine present clear advantages with respect to previous step-detection algorithms used for the analysis of dynamics of motors in in vitro assays when analyzing trajectories of motors or actively transported cargoes in living cells. According to the data showed in Fig. 2 the performance of the step-finder algorithm is slightly worst with respect to that of the Kerssemakers method [39] in conditions in which the dwell period is significantly higher than the sampling time.

The step-finder algorithm is included in the program Cris2011 (Correct RetrIeval of Steps) which can be downloaded from the website (http://www.gdti.df.uba.ar/). The program runs within a Matlab environment (The Mathworks, Natick, MA), and it also contains a code designed for the simulation of 2D trajectories of particles moving in steps with $L$ and $D_T$ distributions selected by the user. To make the analysis of experimental data easier, we included in the program a filtering routine designed to extract the noise of the trajectories. The algorithm is very simple to implement, the user only needs to input the values of $N_{crit}$, and $\delta$, and the desired confidence threshold. The routine of step detection automatically output a plot of the steps as vectors on the trajectory and the histograms of $D_T$ and $L$.

We showed that the step-finder routine works as well as previous algorithms when analyzing 1D trajectories but it allows extending the analysis to 2D trajectories showing more complex behaviors as those observed in the cellular environment. Trajectories of motors or of cargoes attached to active motors are usually tortuous presenting periods of active transport interspersed by periods of diffusion or complex motion that cannot be easily interpreted. Therefore, it is sometimes very difficult to determine an overall direction of the organelle and to distinguish periods of clear active transport to obtain the typical distance vs. time plot required in previous step-detection algorithms. Moreover, analyzing only a small segment of a trajectory may constitute a disadvantage since we may be loosing valuable information to get a more complete view of how transport develops in cells.

It is important to mention that the program considers that $\sigma$ is constant along the analyzed trajectories. In the particular case of the melanosome trajectories analyzed in this study, we studied the dependence of $\sigma$ with time and verified that this approximation is valid (not shown). However, this may not be true in other experimental conditions; for example, the time evolution of the organelle thermal jittering may be relevant when sampling the trajectory at high frequencies. We normally test the consistency of the output of the step-detection algorithm by re-running the program using a slightly different value of $\delta$: it is expected that the output will not change significantly if $\sigma$ was correctly estimated.

The algorithm presented in this study does not require the assumption of a constant step size as it is required, for example, in pair-wise analysis. This is very important because it has been demonstrated that transport of big organelles usually requires the simultaneous action of a small ensemble of motors (see for example, [34, 45]) and peaks observed in this analysis blurred out when multiple motors transport the cargo [11]. On the other hand, it has been demonstrated that dynein performs steps of variable sizes depending on the load [2] and that tandems of motors working together present fractional steps in in vitro assays [11]. A deep analysis of the properties of transport driven by multiple motor have been further explored by Jamison et al. [12] who characterized the properties of motor assemblies composed by two kinesin-1 motors.

The proposed step-finder routine could be used in these cases to analyze whether these properties are conserved in living cells helping to unravel the molecular mechanisms of motors in their natural context.

**Acknowledgments** We are grateful to Marileen Dogterom and Jacob Kerssemakers for kindly providing us with the MatLab code of the $\chi^2$ method. We also thank Dr. Mariela Sued and Dr. Daniela Rodríguez for their useful comments on dwell time distributions. This research was supported by ANPCyT (PICT 2008-1104) and UBACyT (20020090200201). LB and VL are members of CONICET.

## References

1. Gennerich, A., & Vale, R. D. (2009). Walking the walk: How kinesin and dynein coordinate their steps. *Current Opinion in Cell Biology, 21*, 59–67.
2. Mallik, R., Carter, B. C., Lex, S. A., King, S. J., & Gross, S. P. (2004). Cytoplasmic dynein functions as a gear in response to load. *Nature, 427*, 649–652.
3. Toba, S., Watanabe, T. M., Yamaguchi-Okimoto, L., Toyoshima, Y. Y., & Higuchi, H. (2006). Overlapping hand-over-hand mechanism of single molecular motility of cytoplasmic dynein.

*Proceedings of the National academy of Sciences of the United States of America, 103*, 5741–5745.
4. Visscher, K., Schnitzer, M. J., & Block, S. M. (1999). Single kinesin molecules studied with a molecular force clamp. *Nature, 400*, 184–189.
5. Mehta, A. D., Rock, R. S., Rief, M., Spudich, J. A., Mooseker, M. S., & Cheney, R. E. (1999). Myosin-V is a processive actin-based motor. *Nature, 400*, 590–593.
6. Svoboda, K., & Block, S. M. (1994). Force and velocity measured for single kinesin molecules. *Cell, 77*, 773–784.
7. Block, S. M., Asbury, C. L., Shaevitz, J. W., & Lang, M. J. (2003). Probing the kinesin reaction cycle with a 2D optical force clamp. *Proceedings of the National academy of Sciences of the United States of America, 100*, 2351–2356.
8. Yildiz, A., Forkey, J. N., McKinney, S. A., Ha, T., Goldman, Y. E., & Selvin, P. R. (2003). Myosin V walks hand-over-hand: Single fluorophore imaging with 1.5-nm localization. *Science, 300*, 2061–2065.
9. Yildiz, A., Tomishige, M., Vale, R. D., & Selvin, P. R. (2004). Kinesin walks hand-over-hand. *Science, 303*, 676–678.
10. Campas, O., Leduc, C., Bassereau, P., Casademunt, J., Joanny, J. F., & Prost, J. (2008). Coordination of kinesin motors pulling on fluid membranes. *Biophysical Journal, 94*, 5009–5017.
11. Leduc, C., Ruhnow, F., Howard, J., & Diez, S. (2007). Detection of fractional steps in cargo movement by the collective operation of kinesin-1 motors. *Proceedings of the National academy of Sciences of the United States of America, 104*, 10847–10852.
12. Jamison, D. K., Driver, J. W., Rogers, A. R., Constantinou, P. E., & Diehl, M. R. (2010). Two kinesins transport cargo primarily via the action of one motor: Implications for intracellular transport. *Biophysical Journal, 99*, 2967–2977.
13. Ali, M. Y., Krementsova, E. B., Kennedy, G. G., Mahaffy, R., Pollard, T. D., Trybus, K. M., et al. (2007). Myosin Va maneuvers through actin intersections and diffuses along microtubules. *Proceedings of the National academy of Sciences of the United States of America, 104*, 4332–4336.
14. Gagliano, J., Walb, M., Blaker, B., Macosko, J. C., & Holzwarth, G. (2010). Kinesin velocity increases with the number of motors pulling against viscoelastic drag. *European Biophysics Journal, 39*, 801–813.
15. Caspi, A., Granek, R., & Elbaum, M. (2002). Diffusion and directed motion in cellular transport. *Physical Review E, 66*, 011916.
16. Chang, L., Barlan, K., Chou, Y. H., Grin, B., Lakonishok, M., Serpinskaya, A. S., et al. (2009). The dynamic properties of intermediate filaments during organelle transport. *Journal of Cell Science, 122*, 2914–2923.
17. Kulic, I. M., Brown, A. E. X., Kim, H., Kural, C., Blehm, B., Selvin, P. R., et al. (2008). The role of microtubule movement in bidirectional organelle transport. *Proceedings of the National academy of Sciences of the United States of America, 105*, 10011–10016.
18. Brunstein, M., Bruno, L., Desposito, M., & Levi, V. (2009). Anomalous dynamics of melanosomes driven by myosin-V in Xenopus laevis melanophores. *Biophysical Journal, 97*, 1548–1557.
19. Schliwa, M., & Woehlke, G. (2003). Molecular motors. *Nature, 422*, 759–765.
20. Kashina, A. S., Semenova, I. V., Ivanov, P. A., Potekhina, E. S., Zaliapin, I., & Rodionov, V. I. (2004). Protein kinase A, which regulates intracellular transport, forms complexes with molecular motors on organelles. *Current Biology, 14*, 1877–1881.
21. Cai, D., Kaul, N., Lionberger, T. A., Wiener, D. M., Verhey, K. J., & Meyhofer, E. (2010). Recording single motor proteins in the cytoplasm of mammalian cells. *Methods in Enzymology, 475*, 81–107.
22. Kural, C., Kim, H., Syed, S., Goshima, G., Gelfand, V. I., & Selvin, P. R. (2005). Kinesin and dynein move a peroxisome in vivo: A tug-of-war or coordinated movement? *Science, 308*, 1469–1472.
23. Levi, V., Gelfand, V. I., Serpinskaya, A. S., & Gratton, E. (2006). Melanosomes transported by myosin-V in Xenopus melanophores perform slow 35 nm steps. *Biophysical Journal, 90*, L7–L9.
24. Nan, X., Sims, P. A., Chen, P., & Xie, X. S. (2005). Observation of individual microtubule motor steps in living cells with endocytosed quantum dots. *Journal of Physical Chemistry B, 109*, 24220–24224.
25. Watanabe, T. M., & Higuchi, H. (2007). Stepwise movements in vesicle transport of HER2 by motor proteins in living cells. *Biophysical Journal, 92*, 4109–4120.
26. Nan, X., Sims, P. A., & Xie, X. S. (2008). Organelle tracking in a living cell with microsecond time resolution and nanometer spatial precision. *ChemPhysChem, 9*, 707–712.
27. Courty, S., Luccardini, C., Bellaiche, Y., Cappello, G., & Dahan, M. (2006). Tracking individual kinesin motors in living cells using single quantum-dot imaging. *Nano Letters, 6*, 1491–1495.
28. Pierobon, P., Achouri, S., Courty, S., Dunn, A. R., Spudich, J. A., Dahan, M., et al. (2009). Velocity, processivity, and individual steps of single myosin V molecules in live cells. *Biophysical Journal, 96*, 4268–4275.
29. Nelson, S. R., Ali, M. Y., Trybus, K. M., & Warshaw, D. M. (2009). Random walk of processive, quantum dot-labeled myosin Va molecules within the actin cortex of COS-7 cells. *Biophysical Journal, 97*, 509–518.
30. Cai, D., Verhey, K. J., & Meyhofer, E. (2007). Tracking single kinesin molecules in the cytoplasm of mammalian cells. *Biophysical Journal, 92*, 4137–4144.
31. Carter, B. C., Vershinin, M., & Gross, S. P. (2008). A comparison of step-detection methods: how well can you do? *Biophysical Journal, 94*, 306–319.
32. Rogers, S. L., Tint, I. S., Fanapour, P. C., & Gelfand, V. I. (1997). Regulated bidirectional motility of melanophore pigment granules along microtubules in vitro. *Proceedings of the National academy of Sciences of the United States of America, 94*, 3720–3725.
33. Gross, S. P., Tuma, M. C., Deacon, S. W., Serpinskaya, A. S., Reilein, A. R., & Gelfand, V. I. (2002). Interactions and regulation of molecular motors in Xenopus melanophores. *Journal of Cell Biology, 156*, 855–865.
34. Levi, V., Serpinskaya, A. S., Gratton, E., & Gelfand, V. (2006). Organelle transport along microtubules in Xenopus melanophores: Evidence for cooperation between multiple motors. *Biophysical Journal, 90*, 318–327.
35. Scott, D. W. (1979). On optimal and data-based histograms. *Biometrika, 3*, 605–610.
36. Raupach, C., Paranhos Zitterbart, D., Mierke, C., Metzner, C., Muller, F. A., & Fabry, B. (2007). Stress fluctuations and motion of cytoskeletal-bound markers. *Physical Review E, 76*, 011918.
37. Bruno, L., Salierno, M., Wetzler, D. E., Desposito, M. A., & Levi, V. (2011). Mechanical properties of organelles driven by microtubule-dependent molecular motors in living cells. *PLoS One, 6*, e18332.
38. Thompson, R. E., Larson, D. R., & Webb, W. W. (2002). Precise nanometer localization analysis for individual fluorescent probes. *Biophysical Journal, 82*, 2775–2783.
39. Kerssemakers, J. W., Munteanu, E. L., Laan, L., Noetzel, T. L., Janson, M. E., & Dogterom, M. (2006). Assembly dynamics of microtubules at molecular resolution. *Nature, 442*, 709–712.
40. Guo, S., Hong, L., Akhremitchev, B., & Simon, J. D. (2008). Surface elastic properties of human retinal pigment epithelium melanosomes. *Photochemistry and Photobiology, 84*, 671–678.

41. Coles, S. (2001). *An introduction to statistical modeling extreme values*. London: Springer.
42. Gao, X., Yang, L., Petros, J. A., Marshall, F. F., Simons, J. W., & Nie, S. (2005). In vivo molecular and cellular imaging with quantum dots. *Current Opinion in Biotechnology, 16*, 63–72.
43. Fukuda, M., & Kuroda, T. S. (2002). Slac2-c (synaptotagmin-like protein homologue lacking C2 domains-c), a novel linker protein that interacts with Rab27, myosin Va/VIIa, and actin. *Journal of Biological Chemistry, 277*, 43096–43103.
44. Snider, J., Lin, F., Zahedi, N., Rodionov, V., Yu, C. C., & Gross, S. P. (2004). Intracellular actin-based transport: how far you go depends on how often you switch. *Proceedings of the National Academy of Sciences of the United States of America, 101*, 13204–13209.
45. Gross, S. P., Vershinin, M., & Shubeita, G. T. (2007). Cargo transport: two motors are sometimes better than one. *Current Biology, 17*, R478–R486.